UC Berkeley
UC Berkeley Previously Published Works

Title

Codesign of an integrated metal—insulator—semiconductor photocathode for photoelectrochemical reduction of CO 2 to ethylene

Permalink

https://escholarship.org/uc/item/2dh315mc

Journal

Energy & Environmental Science, 16(7)

ISSN

1754-5692

Authors

Kim, Chanyeon

King, Alex J

Aloni, Shaul

et al.

Publication Date

2023-07-12

DOI

10.1039/d2ee03525a

Copyright Information

Peer reviewed

Codesign of an Integrated Metal-Insulator-Semiconductor Photocathode for Photoelectrochemical Reduction of CO₂ to Ethylene

Chanyeon Kim[1,2,3,6], Alex J. King[1,2,3], Shaul Aloni[2,4], Francesca M. Toma[2,3], Adam Z. Weber[2,5], and Alexis T. Bell[1,2,3]*

[1]Department of Chemical and Biomolecular Engineering, University of California, Berkeley, California 94720.

[2]Liquid Sunlight Alliance, Lawrence Berkeley National Laboratory, Berkeley, California 94720.

[3]Chemical Sciences Division, Lawrence Berkeley National Laboratory, Berkeley, California 94720.

[4]The Molecular Foundry, Lawrence Berkeley National Laboratory, Berkeley, California 94720.

[5]Energy Technologies Area, Lawrence Berkeley National Laboratory, Berkeley, California 94720.

[6]Department of Energy Science & Engineering, Daegu Gyeongbuk Institute of Science and Technology, Daegu 42988, Republic of Korea

*Correspondence to: alexbell@berkeley.edu (A.T. Bell)

Abstract

Photoelectrochemical carbon-dioxide reduction (PEC CO_2R) is a potentially attractive means for producing chemicals and fuels using sunlight, water, and carbon dioxide; however, this technology is in its infancy. To date, most studies of PEC CO_2R have reported products containing one carbon atom (C_1 products) but the production of valuable products containing two or more carbons (C_{2+} products), such as ethylene, ethanol, etc., is rarely demonstrated. Metal-semiconductor-insulator (MIS) photocathode/catalyst structures offer a promising approach for this purpose, since they integrate the functions of light absorption, charge separation, and catalysis. In this study, we have investigated a Cu/TiO_2/p-Si photocathode/catalyst structure with the aim of establishing the effects of semiconductor-insulator interactions on the performance of the photocathode and the influence of the direction of illumination of the MIS structure on the total current density and the distribution of products formed by on the Cu catalyst. We have also examined the influence of ionomer coatings deposited on the Cu surface on the total current density and the distribution of products formed. A major finding is that for a fixed Cu potential the distribution of products formed by PEC CO_2R are the same, irrespective of the direction of illumination, and are identical to those obtained by electrochemical reduction of CO_2 (EC CO_2R). Another important finding is that the total current density and the faradaic efficiency to ethylene are enhanced significantly by deposition of a thin bilayer of Sustainion/Nafion onto the surface of the Cu.

Broader Context

The climate crisis resulting from the accumulation of atmospheric CO_2 has motivated growing interest in the conversion of CO_2 to fuels and chemicals using renewable sources of energy (*e.g.*, wind and solar radiation). One approach for doing so is photoelectrochemical carbon dioxide reduction (PEC CO_2R), a process that can directly reduce CO_2 to useful compounds using only water and sunlight. If CO_2 can be captured from the atmosphere, such a process could provide a sustainable source of carbon-

40 based fuels. To date, however, the design principles for successful integration of light absorption, charge

41 separation, and catalyst components of a PEC device are not well understood. This work investigates

42 the co-design of a metal-insulator-semiconductor (MIS) photocathode/catalyst system with the aim of

43 demonstrating how the system elements should be chosen in order to achieve a high selectivity and

44 current density to ethylene via PEC CO_2R. The knowledge gained here also provides insights directly

45 applicable to other PEC systems.

Introduction

Solar production of carbon-containing fuels envisions the direct conversion of solar radiation, carbon dioxide, and water to produce gaseous or liquid fuels.[1-4] This idea is particularly attractive if the carbon dioxide can be sourced from the atmosphere, since it would enable a circular carbon economy. Most previous studies of PEC CO_2R have demonstrated only small amounts of C_1 products, such as CO, CH_4, HCOOH, etc.,[5-7] rather than more valuable multi-carbon (C_{2+}) products.[8, 9] Therefore, it is important to develop a fundamental understanding of how the interplay between the components of a PEC CO_2R photocathode/catalyst structure interact, and how these interactions can be best utilized to achieve high yields of products such as C_2H_4 and C_2H_5OH. These products are targeted because they can be converted to higher molecular weight, preferably liquid, hydrocarbons and alcohols that have high volumetric and mass energy densities.[8, 10, 11]

A key challenge for the development of a PEC CO_2R system is the susceptibility of most photo-absorbers to chemical corrosion and photodegradation in the presence of an electrolyte.[5-7, 12, 13] Moreover, the best photocathodes are poor catalysts for the reduction of CO_2.[13, 14] These issues have led researchers to explore metal-insulator-semiconductor (MIS) structures as photocathodes.[15-20] The metal layer improves reaction kinetics by lowering the overpotential required to achieve a given current density.[14] Photocathode degradation can be inhibited by covering the surface of the semiconductor with a very thin, corrosion-resistant, insulating layer, such as a metal oxide.[17] The insulating layer also serves as a carrier-selective tunneling contact, which helps to mitigate carrier recombination in the metal layer and improve product formation rates. The role of the protective (insulating) layer in MIS structures has recently been explored for PEC water splitting;[16, 18, 21-23] however, in most studies of PEC CO_2R, the role of the insulating film has been underexplored and limited to its effect as a passivation layer.[19, 24, 25] We note further that MIS structures have great potential for PEC CO_2R to C_{2+} products if the semiconductor, insulating layer, and catalyst material can be selected and adapted to each other (*i.e.*, co-designed) to achieve high photovoltage and current, as well as a high faradaic efficiency to

4

71 ethylene.[19-21, 24]

72   The reaction microenvironment near the catalyst surface is also vitally important. Extensive

73 studies have revealed that Cu-based catalysts are best suited for the formation of C_{2+} products[26-28] and

74 that the morphology of the Cu surface, electrolyte cation identity, and the local pH of the electrolyte in

75 contact with the catalyst surface influence both its activity and selectivity for CO_2R.[29-31] Recent work

76 has also demonstrated that the activity and selectivity of Cu for producing C_{2+} products can be enhanced

77 significantly by using thin ionomer films in order to enhance the pH and the CO_2/H_2O ratio at the

78 catalyst surface.[30] A further question is whether an MIS structure using Cu as the catalyst should be

79 illuminated from its dry-side or its wet-side, the side in contact with the electrolyte. Prior work on PEC

80 water splitting has shown that dry-side and wet-side illumination can produce differences in the transfer

81 and utilization of absorbed light energy.[32, 33]

82   The aim of the present study was to understand how the semiconductor-insulator interactions

83 in an MIS structure affect the photovoltage and photocurrent available to drive PEC CO_2R. To this end,

84 we conducted a systematic investigation of the role of each component in a $Cu/TiO_2/p-Si$ MIS structure.

85 Because of the close interactions of the different elements of an MIS structure, it is useful to first identify

86 the relationships among the elements, which are illustrated in Figure 1. The semiconductor light

87 absorber is p-doped silicon (p-Si), a commonly available material that has been investigated previously

88 for PEC applications. Cu catalyst was chosen as the catalyst because it exhibits the ability to catalyze

89 the electrochemical reduction of CO_2 to C_{2+} products with high faradaic efficiency.[26-28] TiO_2 was used

90 as the protective layer for p-Si because it is known to be stable in aqueous electrolytes.[17, 34] Figure 1

91 also shows that TiO_2 and p-Si have a low conduction band offset and a large valence band offset.[35]

92 These are important characteristics for achieving carrier selective tunneling, which is exponentially

93 dependent on the band offset between the semiconductor and insulator. A larger band offset results in a

94 lower tunneling probability and, consequentially, a lower rate of carrier tunneling. Thus, a TiO_2

95 insulating layer is well suited for protecting the semiconductor and enabling facile tunneling of the

96 desired charge (electrons) due to its high tunneling probability. The tunneling probability is also

97 exponentially dependent on the thickness of the insulator; hence, the TiO_2 layer must be thin enough to

98 allow electron tunneling through it to the metal layer, but thick enough to protect the semiconductor

99 and limit hole tunneling.[36-38] Therefore, an optimum TiO_2 thickness is expected in order to achieve high

100 photovoltages.[15, 17] We note that an understanding of how the thickness of the TiO_2 layer alters the

101 environment at the semiconductor surface, and, subsequently, the photovoltage, is not currently known.
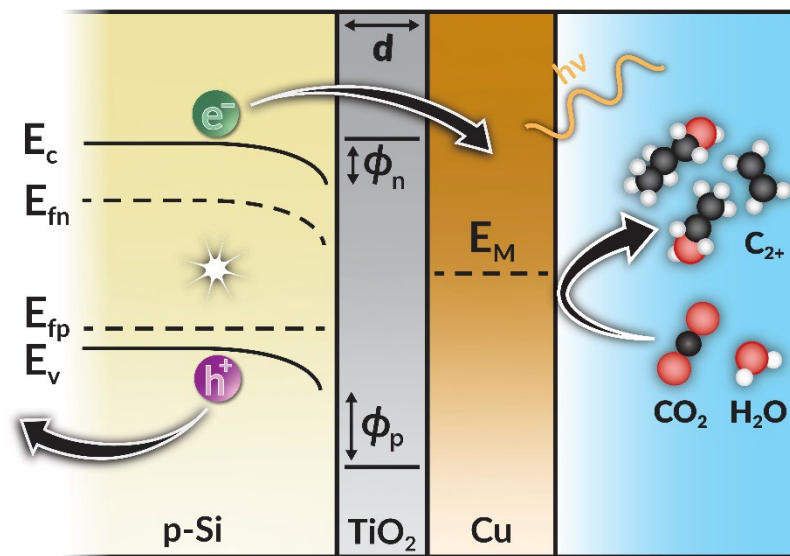
102

103 **Figure 1. Band diagram illustration of an MIS photocathode converting CO_2 to C_2 products.** Electrons can
104 easily tunnel into the Cu layer because of the small barrier (ϕ_n), whereas hole tunneling is blocked by the large
105 barrier (ϕ_p). d is the thickness of the TiO_2 layer. E_c and E_v are the conduction and valence bands, respectively. E_{fn},
106 E_{fp}, and E_M are the electron and hole quasi-Fermi level, respectively, and the metal Fermi level.
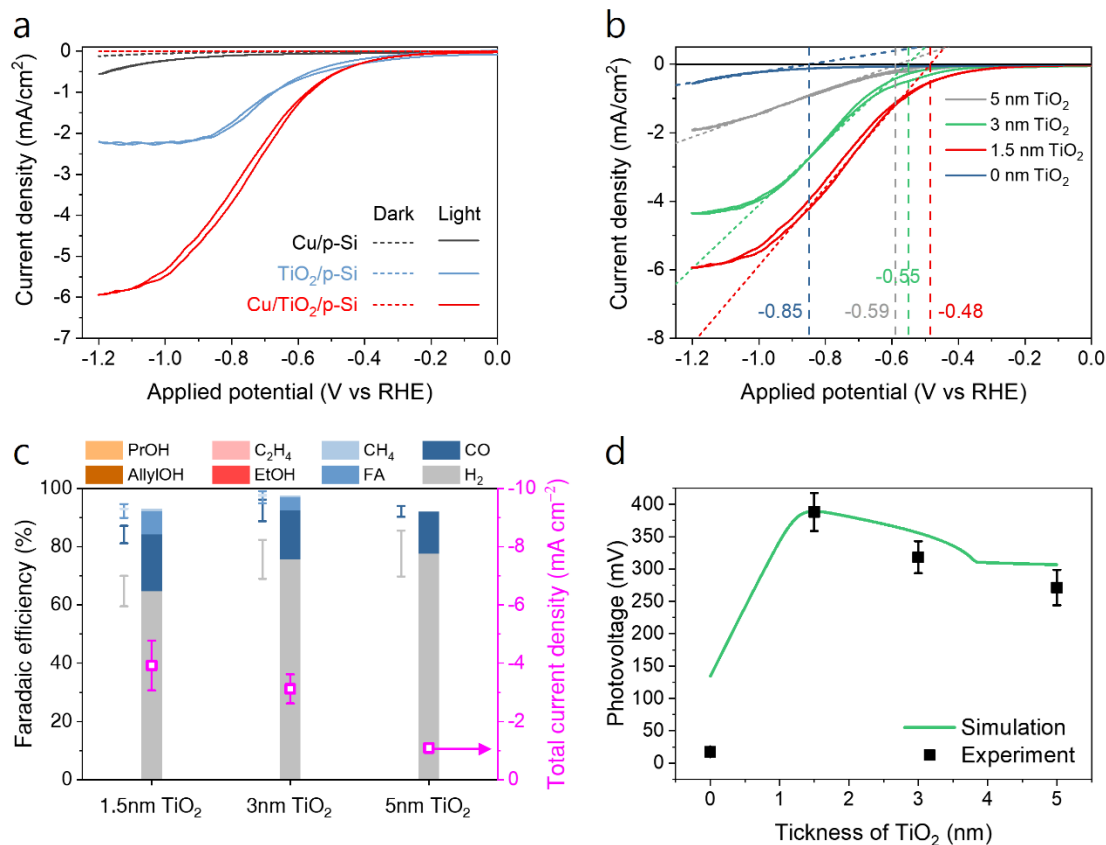
107

108

109

110

111

112 **Results and Discussion**

The effects of each component of a Cu/TiO$_2$/p-Si MIS structure on the total current density, photovoltage, and product Faradaic efficiencies for PEC CO$_2$R

Figure 2. The effect and role of each component in the MIS photocathode. a. response in photocurrent during CV using various configurations of photocathode in CO$_2$R environments under dry-side illumination, b. photocurrent obtained during CV, c. product distribution obtained during CA at −0.9 V vs RHE, and d. comparison of the theoretical and experimentally measured photovoltage with respect to the thickness of TiO$_2$ insulator layer in in Cu/TiO$_2$/p-Si MIS photocathode at zero current density. In a-c, PEC CO$_2$R was conducted in the presence of 0.1 M CsHCO$_3$ electrolyte.

Figure 2 illustrates the effect of each component comprising the MIS photocathode on the current density for a given applied voltage. Cyclovoltammetry (CV) data were collected using a compression cell with two symmetric anodic chambers placed perpendicular to the cathode chamber (see Figure 3a, below)[39] for different photocathode configurations under conditions of no illumination (dark) and dry-side illumination (Figure 2a), *i.e.*, the side that is not exposed to the electrolyte (also referred elsewhere as back-side). We note that bare p-Si has been previously shown to be a poor CO$_2$R catalyst and primarily evolves H$_2$;[14] hence, our investigation first examined Cu on p-type silicon (Cu/p-

129 Si), to improve CO_2R activity. Cu/p-Si exhibited only a slight increase in total current density

130 (photocurrent) under dry-side illumination, denoted by the black solid line, compared to that obtained

131 under dark conditions (dark current), denoted by dotted black line. This minor increase in current

132 density under dry-side illumination is due to significant Fermi-level pinning of Cu and p-Si.[36-38]

133   When a thin layer of TiO_2 is used to passivate p-Si (TiO_2/p-Si), the photocurrent increases

134 noticeably (blue solid line) due to improved carrier transport and defect-passivation of the insulating

135 TiO_2 layer, whereas the dark current is similar to that obtained for Cu/p-Si. The principal product for

136 TiO_2/p-Si, however, is H_2 (Figure S1). Interestingly, the photocurrent can be further increased with an

137 additional Cu layer (Cu/TiO_2/p-Si MIS, red line) due to the increase in CO_2R activity relative to that for

138 TiO_2/p-Si. These observations clearly demonstrate the role of each component. Although the TiO_2 layer

139 only produces H_2, it enhances the photocurrent and photovoltage obtained from p-Si as a consequence

140 of its effects on carrier tunneling and surface passivation. The effect of the TiO_2 layer can be varied by

141 changing its thickness, which in turn affects the carrier-tunneling probabilities.[16, 18, 21] As the TiO_2 layer

142 thickness decreases from 5 nm, not only the photocurrent but also the photovoltage increases. The

143 photovoltage was estimated by the shift in potential at which current flow begins (the onset potential)

144 for each MIS photocathode (Figure 2b) and that for electrochemical (EC) CO_2R (Figure S2). The

145 differences in PEC CO_2R performances during chronoamperometry (CA) at -0.9 V vs RHE observed

146 with varying TiO_2 thickness, shown in Figure 2c, is a consequence of differences in generated

147 photovoltages. Our measurements, shown in Figure 2d, indicate a TiO_2 thickness of ~ 1.5 nm leads to

148 the highest photovoltage (~ 400 mV).

149   The effects of TiO_2 thickness on the photovoltage for the Cu/TiO_2/p-Si photocathode structure

150 was modeled in order to explain why a maximum in the photovoltage occurs at a particular insulator

151 thickness. An overview of this effort is presented in the Supporting Information; specific details can be

152 found elsewhere.[40] This work reveals that with increasing insulator thickness, the electron-tunneling

153 probability decreases (Figure S3) due to an attenuation of the electron wavefunction. The lowered

154 tunneling probability increases the resistances to electron transport across the MIS interface, which, in

8

155 turn, leads to a buildup of electrons near the semiconductor surface. This buildup of electrons occurs

156 for TiO_2 thicknesses $\lesssim$ 1.5 nm, beyond which the electron concentration decreases; see Figure S4. This

157 decrease in electron concentration occurs because of a high bulk and interfacial recombination rate, as

158 seen in Figure S5, which is attributable to the large electron concentration and density of interfacial trap

159 sites. The electron concentration at the semiconductor surface alters the quasi-Fermi level of electrons,

160 and, consequentially, the photovoltage (for details the reader is referred to the Supporting Information

161 and Figure S4); the band energy diagram at varying TiO2 thicknesses is shown in Figure S6. Thus, the

162 increase in photovoltage for TiO_2 films $\lesssim$ 1.5 nm thick is due to the increase in electron concentration,

163 whereas the decrease in electron concentration for TiO_2 thicknesses > 1.5 nm causes the reduction in

164 photovoltage. We note that the effects of quantum confinement in the TiO_2 layer on the simulation

165 results are negligible, as shown in Figure S7. Notwithstanding the discrepancies observed in the absence

166 of a TiO_2 layer and for thick TiO_2 layers, Figure 2d shows that the theoretical predictions capture the

167 experimental trends in photovoltage with insulator thickness quite effectively, especially at thicknesses

168 relevant to this study.

169 **The effects of dry-side vs wet-side illuminations on the performance of a Cu/TiO$_2$/p-Si MIS**

170 **structure**

171 The MIS architecture of the photocathode is geometrically asymmetric; therefore, the

172 questions arises whether the performance of the MIS structure will differ when it is illuminated from

173 the dry- vs the wet-side. This question was investigated using the compression cell shown in Figure 3a

174 (see the Experimental Methods section for more details).[39] To evaluate the effect of light in terms of the

175 electric potential at the Cu surface, where CO_2R occurs, an electric contact was made on the wet-side

176 as well as through an Al/Au ohmic contact located on the dry-side of the MIS photocathode (see Figure

177 3b). Prior to using the MIS photocathode for PEC CO_2R under wet-side illumination, the light

178 transmission through the Cu and TiO_2 layers was measured. As shown in Figure S8a, incident light

179 transmission through 1.5 nm of TiO_2 was > 90 % for wavelengths from 350 to 1500 nm. However, when

180 a Cu layer was deposited on top of the TiO_2 layer, light transmission decreased noticeably from < 80 %

181 to below 55 % as the thickness of the Cu layer increased from 10 to 25 nm. As shown in Figure S8b, a

182 decrease in light transmission leads to a decrease in the photocurrent. When the Cu thickness was 10

183 nm, the hydrogen evolution reaction (HER) dominated over CO_2R, most likely due to partial exposure

184 of the TiO_2 layer below the Cu. These results indicate that a Cu thickness of 15 nm is optimal in order

185 to reduce the loss of light transmission, while concurrently promoting CO_2R selectivity; hence, 15 nm

186 was used in all subsequent experiments.
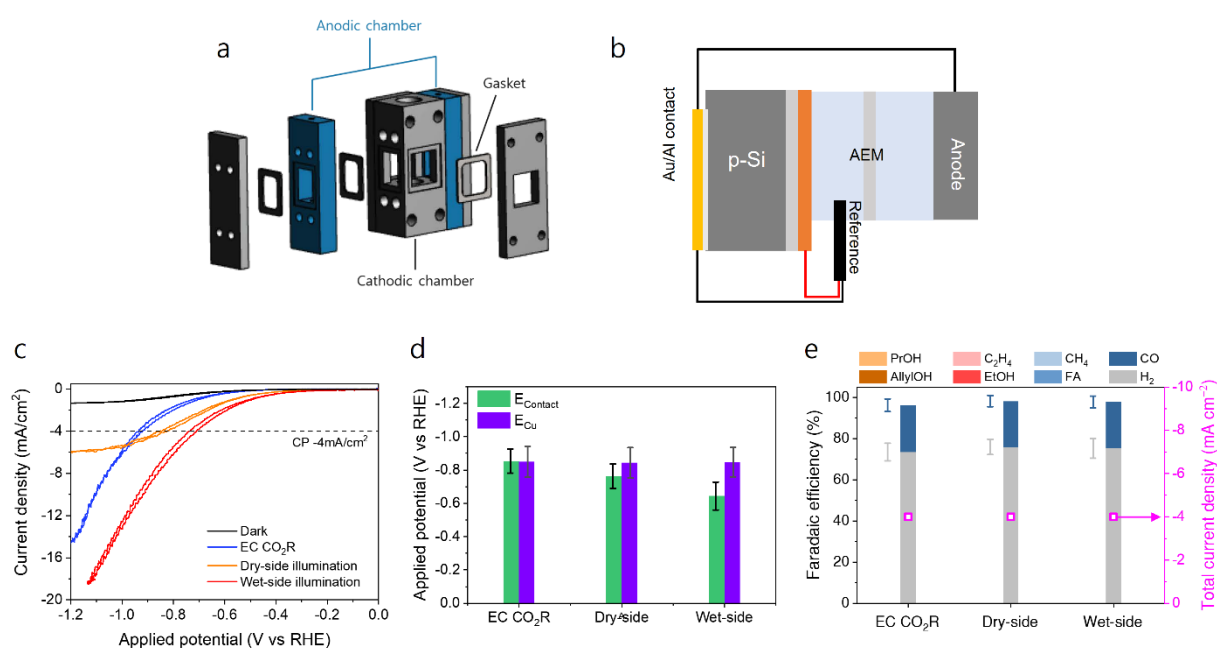
187

188 **Figure 3. PEC CO_2R using MIS photocathode under dry-side and wet-side illuminations.** Schematic
189 illustration of **a.** PEC cell enabling both dry-side and wet-side illumination and **b.** configuration of electric circuit.
190 **c.** CV curves obtained using MIS photocathode under various conditions of EC CO_2R, dark, dry-side and wet-
191 side illumination. Effect of illuminating direction on **d.** potential measured at Cu surface and **e.** product
192 distribution during PEC CO_2R using MIS photocathode at constant current density of $-4mA/cm^2$. In **c-e**, PEC
193 CO_2R was conducted in the presence of 0.1 M $CsHCO_3$ electrolyte.

194 Under dry-side illumination the photovoltage and photocurrent is generated solely by light

195 absorption from p-Si; under wet-side illumination, however, the light passes through all three layers

196 (Cu, TiO_2, and p-Si). Therefore, the effect of light with respect to the direction of illumination needs to

197 be investigated in terms of both photocurrent and photovoltage in order to ascertain the effects of light

198 absorption and reflection by the Cu and TiO_2 layers. Figure 3c shows CV data acquired for dry-side and

wet-side illumination of the MIS photocathode/catalyst as well as for EC CO_2R, which use identical Cu

catalysts. In the case of EC CO_2R, the potential was applied between the Cu surface in MIS

photocathode/catalyst and the reference electrode using a potentiostat. Interestingly, the photocurrent

obtained under wet-side illumination (red line) was noticeably higher than that obtained under dry-side

illumination (orange line), even though partial light absorption and reflection by the Cu and TiO_2 layers

occurred in the latter case. This observation implies there is better utilization of absorbed photons under

wet-side illumination compared to dry-side illumination. To validate this hypothesis, a potential was

applied to the p-Si (at the Au/Al contact on the dry-side) and the potential at the Cu layer on the wet-

side was measured during chronopotentiometry (CP) at $-$ 4 mA/cm^2 (Figure 3d). While the potential

measured at the Cu surface was identical for all cases (purple columns), there were differences in the

potential applied by the potentiostat, indicating that the electric potential required to reach $-$ 4 mA/cm^2

was different for EC CO_2R and PEC CO_2R under dry-side and wet-side illumination (green columns).

The required applied potential to reach a current density of $-$ 4mA/cm^2 was $-$ 0.76 V and $-$ 0.64 V vs

RHE for dry-side and wet-side illumination, respectively. The additional 120 mV of photovoltage under

wet-side illumination compared to dry-side illumination is a result of the improved charge utilization.

For a nearly identical potential at the Cu surface, around $-$ 0.84 V vs RHE, the product distributions

obtained for EC CO_2R and PEC CO_2R under wet-side and dry-side illumination were nearly identical
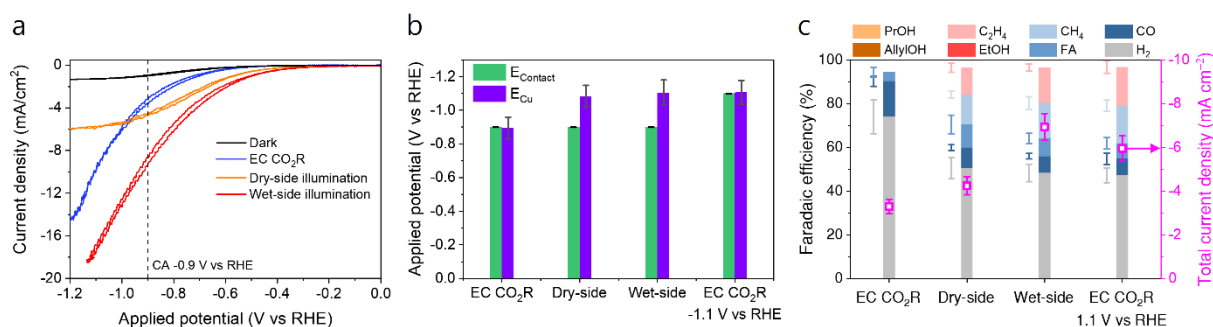
(Figure 3e).

Figure 4. PEC CO_2R using MIS photocathode under dry-side and wet-side illuminations at constant potential condition of $-$0.9 V vs RHE. a. CV curves obtained using MIS photocathode under various conditions of EC CO_2R, dark, dry-side and wet-side illumination. Effect of illuminating direction on **b.** potential measured

11

221 at Cu surface under the constant applied potential of -0.9V vs RHE to p-Si with respect to the reference electrode
222 and **c.** product distribution. In **a-c**, PEC CO_2R was conducted in the presence of 0.1 M $CsHCO_3$ electrolyte.

223   The effects of dry-side and wet-side illumination were also investigated at a constant applied

224 potential of -0.9 V vs RHE, shown in Figure 4a in order to further support our hypothesis of enhanced

225 charge utilization under wet-side illumination. Although the potential applied by the potentiostat (green

226 columns) was the same, the potential at the Cu surface decreased from -0.89 to -1.07 to -1.10 V vs

227 RHE for EC CO_2R, PEC CO_2R under dry-side illumination, and PEC CO_2R under wet-side illumination,

228 respectively (Figure 4b). As a consequence of the larger negative potential at the Cu surface, PEC CO_2R

229 under dry-side and wet-side illumination exhibited increased current density for CO_2R vs HER and,

230 more importantly, formation of ethylene. When the potential at the Cu surface was similar for PEC

231 CO_2R under wet-side illumination and EC CO_2R (-1.10 V vs RHE), the product faradaic efficiencies

232 were similar as well (Figure 4c). Thus, the effect of light is to reduce the potential required by the

233 potentiostat to maintain the Cu potential around -1.10 V vs RHE. It is important to note that PEC CO_2R

234 under dry-side illumination produced a saturated current response, reaching a plateau at around -7

235 mA/cm^2 at -1.2 V vs RHE as shown in Figure 4a. This plateau in current density is not related to either

236 mass-transport-limited CO_2R or tunneling resistances of photo-generated charges through the TiO_2 layer

237 because these limitations would also been seen in EC CO_2R and PEC CO_2R under wet-side illumination,

238 respectively. Therefore, saturation of the photocurrent under dry-side illumination is attributed to carrier

239 recombination across the p-Si layer.

240   Similar limitations from carrier recombination has been reported for PEC water splitting.[32, 33,]

241 [41-43] In these studies, wet-side illumination resulted in several fold higher photocurrents than dry-side

242 illumination, in agreement with the findings shown here. The authors of these studies proposed that the

243 diffusion length of charge carriers, which is less than a micron, is much shorter than the thickness of

244 the semiconductor photo-absorber, several hundred microns. Hence, a significant number of excited

245 electrons recombine with holes as they travel across the photo-absorber to the metal surface, resulting

246 in the low photocurrent observed under dry-side illumination. This interpretation is further supported

12

247   by the work of Bae *et al*., who investigated the influence of the thickness of a p^+pn^+-Si photo-absorber

248   on the photocurrent produced during PEC water splitting under both wet-side and dry-side

249   illumination.[32] They found that the photocurrent under dry-side illumination was $\sim 20\%$ lower than that

250   under wet-side illumination even though the thickness of p^+pn^+-Si was reduced from 350 to 50 μm. The

251   authors attributed this finding to the small ratio of carrier diffusion length to the thickness of the p^+pn^+-

252   Si photo-absorber. Therefore, we conclude that dry-side illumination cannot achieve photocurrents as

253   high as those attained under wet-side illumination unless the carrier diffusion length is improved.

254   **Effects of ionomer coatings on the activity and product selectivity of Cu for PEC CO_2R**

255   Previous studies of EC CO_2R have shown that the microenvironment near the surface of a Cu

256   catalyst plays a critical role in defining its activity and selectivity for producing C_{2+} products. It has

257   been found that a high pH and CO_2/H_2O ratio at the Cu surface promoted the formation of C_{2+} products

258   relative to C_1 products and H_2.[29, 30] We have recently reported that these requirements can be met by

259   coating the surface of Cu with a thin ionomer bilayer. For CO_2R on Nafion/Sustainion/Cu, the

260   Sustainion layer, which is an anion conducting ionomer with high CO_2 affinity, enhances local CO_2

261   concentration near Cu surface; whereas, the Nafion layer, which is a cation conducting ionomer with a

262   negative background charge, causes the accumulation of OH^- through Donnan exclusion.[30]

263   We investigated the effects depositing an ionomer bilayer (Nafion on top of Sustainion) on the

264   surface of Cu in a $Cu/TiO_2/p$-Si MIS structure to see whether the bilayer would enhance the formation

265   of C_{2+} products formed by PEC CO_2R. The loading of each ionomer layer was selected on the basis of

266   the experiments described in the Supporting Information (See Figure S9). The optimal loadings of

267   Nafion on Sustainion/MIS (N/S/MIS) were chosen to be 0.9 μg/cm^2 and 1.8 μg/cm^2, respectively. As

268   seen in in Figure 5a, the N/S/MIS configuration produced a higher photocurrent than that obtained for

269   the uncoated MIS, even though the light flux to the photocathode was 10% lower due to light absorption

270   by the ionomer bilayer (Figure S10). To further investigate the influence of the ionomer coatings on the

271   product distribution, CA was conducted at -0.9 V vs RHE under wet-side illumination. Similar to our

272 previous results, the potential at the Cu surface was about 0.2 V more negative than that applied to the

273 MIS (Figure 5b), which is comparable to the value obtained using the uncoated MIS structure under

274 dry-side and wet-side illuminations. However, due to the high local pH caused by Donnan exclusion

275 from the presence of the Nafion layer, the selectivity to hydrogen and methane, which are pH sensitive

276 products,[44-46] decreased. Concurrently, the total current density increased up to 10 mA/cm^2 because of

277 the high local CO_2 concentration in the Sustainion layer (Figure 5c). The impact of the bilayer ionomer

278 film on MIS performance is more prominent in terms of partial current density because both selectivity

279 and total current density increased. As shown in Figure 5d, PEC CO_2R using the MIS structure under

280 wet-side illumination exhibited a CO_2R partial current density of $-$ 3.1 mA/cm^2 of which the partial

281 current density for ethylene is $-$ 0.9 mA/cm^2. These values increased to $-$ 5.4 mA/cm^2 and $-$ 2.3 mA/cm^2,

282 respectively, by inclusion addition of the ionomer bilayer on Cu catalyst surface. This selectivity

283 towards ethylene is maintained for several hours under sequential dark and illumination conditions, as

284 shown in Figure S11. These observations are notable because EC CO_2R produced a partial current

285 density for CO_2R of only $-$ 0.6 mA/cm^2 without any ethylene formation at an applied potential of $-$ 0.9

286 V vs RHE.
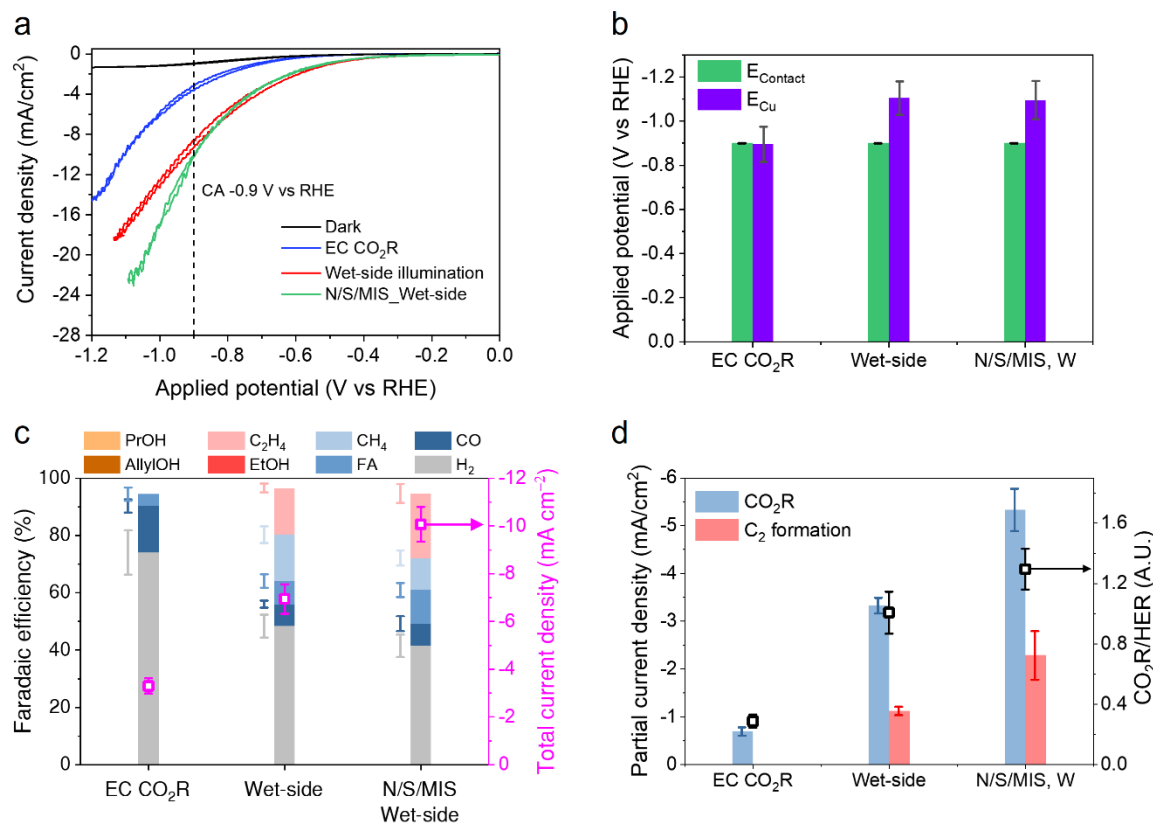
Figure 5. Effect of ionomer bilayer on PEC CO₂R using MIS photocathode. a. Comparison of CV curve obtained using N/S/MIS photocathode with those obtained using pristine MIS under various conditions. **b.** potential measured at Cu surface, **c.** product distribution, and **d.** partial current density for CO_2R and ethylene production during CA -0.9V vs RHE. All the PEC CO_2R was conducted in the presence of 0.1 M $CsHCO_3$ electrolyte.

Conclusions

The present study clearly demonstrates that the performance of a metal-insulator-semiconductor (MIS) photocathode/catalyst structure used for PEC CO_2 in CO_2-saturated 0.1 M $CsHCO_3$ can be tuned by altering the interface between the semiconductor and insulator layers, as well as by the direction of illumination. A thin TiO_2 layer deposited on p-Si improves the photocurrent and photovoltage obtained from the photocathode. This improvement occurs because of a moderate tunneling resistance through the insulating (TiO_2) film, which, in turn, causes a buildup of electrons at the p-Si surface that increases its quasi-Fermi level. Although wet-side illumination of a $Cu/TiO_2/p$-Si MIS photocathode attenuates the flux of light to the photo-absorber, a thin Cu layer (~ 15 nm) deposited

15

303 over the insulator exhibits a substantial increase in the photocurrent relative to dry-side illumination.

304 The observed advantage of wet-side over dry-side illumination is a direct consequence of the low

305 diffusion length of the excited charge carriers, leading to significant carrier recombination; this limits

306 the collection of electrons at the Cu catalyst that subsequently drives CO_2R. The partial current density

307 for CO_2R and that for ethylene production on Cu can be further enhanced by deposition of thin layers

308 of Sustainion and then Nafion over the Cu surface. The bilayer coating increases the partial current for

309 CO_2R, due to the higher solubility of CO_2 in the Sustanion layer, and increases the selectivity to ethylene,

310 due to OH^- exclusion by the Nafion layer, which suppresses the formation of H_2. Under wet-side

311 illumination, the net effect of the ionomer bilayer is that the partial current density of CO_2R is 2.5 times

312 higher and that for ethylene is 4 times higher than that obtained by dry-side illumination of the

313 $Cu/TiO_2/p$-Si MIS photocathode/catalyst structure in the absence of the bilayer coating. The

314 fundamental knowledge gained from the present work can be applied directly to other combinations of

315 metals, insulators, and semiconductors in order to facilitate the unbiased operation of PEC CO_2R for

316 the production of C_{2+} products, as well as other photo-electrosynthetic processes.

317 **Experimental Methods**

318 **Preparation of a $Cu/TiO_2/p$-Si MIS photocathode**

319   Prior to fabricating an MIS photocathode, a 1-10 Ω-cm p-type silicon wafer (boron doped,

320 500µm thickness, <100> orientation, University Wafer Inc.) was rinsed consecutively with acetone

321 ($\geq$99.5%, VWR), isopropyl alcohol (Sigma Aldrich, 99.9%), and methanol ($\geq$99.8%, VWR) for 30 min

322 each. The p-Si wafer was then immersed in 1% HF for 5min to remove the native oxide layer and rinsed

323 with Milli-Q water (18.2MΩ·cm). To make an ohmic contact with the p-Si wafer, it was masked with

324 2-mm wide Kapton tape in order to produce 1 mm of spacings between fingers. Al (99.999% Kurt J.

325 Lesker) and Au (99.999% Kurt J. Lesker) were then sputtered onto the unmasked portions of the wafer.

326 using an AJA ATC Orion-5 magnetron sputtering system on the masked p-Si in order to achieve target

327 thickness of 50 nm for Al and 300 nm for Au. The TiO_2 insulating layer was deposited by atomic layer

328   deposition (ALD) on the opposite side to the one with Al/Au contacts. In the ALD process, the

329   deposition chamber was heated to 125°C and Titanium isopropoxide (TTIP, 99.999% trace metals basis,

330   Sigma-Aldrich) was pulsed into the reactor, to form a TiO_2 film, after which water vapor was pulsed

331   into the reactor. This ALD cycle was repeated in order achieve the desired thickness of the insulator

332   layer, with the thickness measured using ellipsometry (α-SE, J.A.Woollam Co., Inc.). After ALD

333   deposition of TiO_2, Cu (99.999% Kurt J. Lesker) was sputtered for different deposition time to change

334   the thickness of the deposited Cu film. For the EC experiments, 15 nm of Cu was sputtered onto p^+-Si

335   at the same conditions as those used for the MIS samples.

336   **Characterization of the MIS photocathode**

337   Cross-sectional images of a fresh 15nm Cu/1.5nm TiO_2/Si sample were obtained with STEM

338   and energy filtered STEM. The STEM image (Figure S12a) shows there are three distinct layers in the

339   MIS sample, and the energy filtered STEM confirms the three layers are Cu on TiO_2 on Si (Figures

340   S12b and c). We also note the presence of the native SiO_2 layer between Si and TiO_2. STEM energy

341   dispersive x-ray spectroscopy (EDS) also confirms these results (Figure S13a and b). We also performed

342   STEM-EDS of the ionomer-bilayer-coated MIS sample, which shows the presence of the Nafion and

343   Sustanion on top of the MIS photocathode (Figure S14).

344   **Coating of ionomer layer on MIS photocathode**

345   Commercial Nafion (Chemours, 850g mol^{-1} equivalent weight (EW), 20wt% dispersion in

346   20wt% N-propanol aqueous solution), and Sustainion (Dioxide Materials, 5% in ethanol) were drop

347   cast onto the Cu/TiO_2/p-Si MIS system. Stock solutions were prepared by diluting the ionomer solution

348   with isopropyl alcohol (Sigma Aldrich, 99.9%). Prepared stock solutions were drop cast to achieve

349   different loading loadings of ionomers and then dried at room temperature for 1h.

350   **Photoelectrochemical CO_2 reduction**

351   PEC CO_2R was performed in a flow-through compression cell shown in Figure 3a.[39] The cell

352   has 3 electrodes – an MIS photocathode, an Ag/AgCl (filled with 3.4M KCl, Leak-Free, Innovative

353   Instruments) reference electrode, and a platinum foil (99.995%, Sigma-Aldrich) counter electrode. The

354   cell has two identical anode chambers located perpendicular to the cathode chamber. All cell

355   components were machined from polyether ether ketone (PEEK). An anion membrane (Selemion AMV,

356   AGC Engineering Co.) was placed in between the cathodic chamber and two anodic chambers. A 0.05M

357   solution of Cs_2CO_3 (99.995%, Sigma-Aldrich) was prepared using Milli-Q water and pretreated to

358   remove metal impurities using chelating agent solution (Chelex 100, Na form, Sigma-Aldrich) prior to

359   being used. The electrolyte was saturated with a flow of CO_2 (20 sccm, 99.999%, Praxair Inc) for 30

360   min in a gas-tight reservoir to obtain 0.1M of $CsHCO_3$ and circulated through the PEC cell using a

361   peristaltic pump (FH100M, Thermo Scientific) at a rate of 80 ml min^{-1}. A solar simulator was used as

362   the light source (300W, 1.5 A.M., 16S-Series, Solar Light) to obtain a light flux of 100 mW cm^{-2}. The

363   desired flux was achieved by controlling the distance from the light source to the cell and by measuring

364   the local flux using a radiometer (PMA2100, Solar Light). The illuminated area of the MIS

365   photocathode was 1 cm^2 under both dry-side and wet-side illuminations. Electrochemical measurements

366   were performed using a potentiostat (VSP-300, Biologic). An uncompensated resistance (R_u) was

367   determined by both potentiostatic electrochemical impedance spectroscopy (PEIS) and the current

368   interrupt (CI) method and compensated to 85% using the potentiostat. All potentials are shown after

369   conversion to the RHE scale as $E_{RHE} = E_{Ag/AgCl} + 0.197\,V + 0.0591 \times pH$.

Product analysis

371   Gaseous products formed by PEC CO_2R were separated from liquid electrolysis in a gas-tight

372   reservoir and then analyzed by online gas chromatograph (GC) using a gas chromatograph (7890B,

373   Agilent) equipped with a pulsed-discharge helium ionization detector (PDHID) and ShinCarbon ST and

374   Hayesep-Q capillary columns (Agilent); helium (99.9999%, Praxair Inc.) was used as the carrier gas.

375   For quantitative analysis, a calibration curve for each gaseous product was generated by measuring the

18

376 signal for each component obtained by analysis of a series of NIST-traceable standard gas mixtures

377 (100 to 8000 ppm, Airgas Inc.). Liquid products collected in the catholyte reservoir over a period of 30

378 min were analyzed in a high-pressure liquid chromatograph (HPLC) (UltiMate 3000, Thermo Scientific)

379 equipped with Aminex HPX 87-H columns (Bio-Rad Inc.) and a refractive index detector (RID). The

380 signal for each liquid product was quantified using a calibration curve based on a series of standard

381 solutions for each product in the range of concentration from 0.1 to 20 mM. Faradaic efficiency (FE)

382 corresponding to product i was calculated as $FE = \frac{nFc_iV}{I_{total}} \times 100$ %, where n is the number of electrons

383 transferred, F is Faraday's constant, c_i is molar concentration of species i, V is the total volumetric flow

384 rate and I_{total} is the measured total current.

385 **Data availability**

386 All data of this study is available within the article and its Supplementary Information.

387 **Acknowledgments**

397 **Author contributions**

19

398 C.K. performed photocathode preparation, photoelectrochemical experiments,

399 characterizations, and data interpretation. A.J.K. performed theoretical calculations. S.A.

400 conducted chemical and physical characterization of the MIS sample. A.T.B., A.Z.W., and

401 F.M.T. supervised the project. All authors discussed the result and participated in the

402 preparation of the manuscript.

403 **Competing interests**

404 Authors declare no competing interests.

405

406 **References**

407 1. W.-H. Cheng, A. de la Calle, H. A. Atwater, E. B. Stechel and C. Xiang, *ACS Energy Lett.*, 2021,
408   **6**, 3096-3113.
409 2. A. J. King, J. C. Bui, A. T. Bell and A. Z. Weber, *ACS Energy Lett.*, 2022, DOI:
410   10.1021/acsenergylett.2c01041, 2694-2700.
411 3. G. Segev, J. Kibsgaard, C. Hahn, Z. J. Xu, W.-H. Cheng, T. G. Deutsch, C. Xiang, J. Z. Zhang, L.
412   Hammarström, D. G. Nocera, A. Z. Weber, P. Agbo, T. Hisatomi, F. E. Osterloh, K. Domen, F.
413   F. Abdi, S. Haussener, D. J. Miller, S. Ardo, P. C. McIntyre, T. Hannappel, S. Hu, H. Atwater, J.
414   M. Gregoire, M. Z. Ertem, I. D. Sharp, K.-S. Choi, J. S. Lee, O. Ishitani, J. W. Ager, R. R. Prabhakar,
415   A. T. Bell, S. W. Boettcher, K. Vincent, K. Takanabe, V. Artero, R. Napier, B. R. Cuenya, M. T. M.
416   Koper, R. Van De Krol and F. Houle, *J. Phys. D: Appl. Phys.*, 2022, **55**, 323003.
417 4. Q. Wang, C. Pornrungroj, S. Linley and E. Reisner, *Nat. Energy*, 2022, **7**, 13-24.
418 5. J. He and C. Janáky, *ACS Energy Lett.*, 2020, **5**, 1996-2014.
419 6. V. Kumaravel, J. Bartlett and S. C. Pillai, *ACS Energy Lett.*, 2020, **5**, 486-519.
420 7. Y. Liu and L. Guo, *J. Chem. Phys.*, 2020, **152**, 100901.
421 8. S. Nitopi, E. Bertheussen, S. B. Scott, X. Liu, A. K. Engstfeld, S. Horch, B. Seger, I. E. L. Stephens,
422   K. Chan, C. Hahn, J. K. Nørskov, T. F. Jaramillo and I. Chorkendorff, *Chem. Rev.*, 2019, **119**,
423   7610-7672.
424 9. W. Lai, Y. Qiao, J. Zhang, Z. Lin and H. Huang, *Energy Environ. Sci.*, 2022, **15**, 3603-3629.
425 10. S. Verma, B. Kim, H.-R. M. Jhong, S. Ma and P. J. A. Kenis, *ChemSusChem*, 2016, **9**, 1972-
426   1979.
427 11. D. T. Whipple and P. J. A. Kenis, *J. Phys. Chem. Lett.*, 2010, **1**, 3451-3458.

428 12. G. Liu, F. Zheng, J. Li, G. Zeng, Y. Ye, D. M. Larson, J. Yano, E. J. Crumlin, J. W. Ager, L.-w. Wang
429   and F. M. Toma, *Nat. Energy*, 2021, **6**, 1124-1132.

430 13. A. K. Singh, J. H. Montoya, J. M. Gregoire and K. A. Persson, *Nat. Commun.*, 2019, **10**, 443.

431 14. R. Hinogami, Y. Nakamura, S. Yae and Y. Nakato, *J. Phys. Chem. B*, 1998, **102**, 974-980.

432 15. I. A. Digdaya, B. J. Trześniewski, G. W. P. Adhyaksa, E. C. Garnett and W. A. Smith, *J. Phys.*
433   *Chem. C*, 2018, **122**, 5462-5471.

434 16. J. Hemmerling, J. Quinn and S. Linic, *Adv. Energy Mater.*, 2020, **10**, 1903354.

435 17. J. R. Hemmerling, A. Mathur and S. Linic, *Acc. Chem. Res.*, 2021, **54**, 1992-2002.

436 18. J. Quinn, J. Hemmerling and S. Linic, *ACS Energy Lett.*, 2019, **4**, 2632-2638.

437 19. P. Wen, H. Li, X. Ma, R. Lei, X. Wang, S. M. Geyer and Y. Qiu, *J. Mater. Chem. A*, 2021, **9**,
438   3589-3596.

439 20. T. Zhu and M. N. Chong, *Nano Energy*, 2015, **12**, 347-373.

440 21. I. A. Digdaya, G. W. P. Adhyaksa, B. J. Trześniewski, E. C. Garnett and W. A. Smith, *Nat.*
441   *Commun.*, 2017, **8**, 15968.

442 22. S. Lee, L. Ji, A. C. De Palma and E. T. Yu, *Nat. Commun.*, 2021, **12**, 3982.

443 23. P. P. Sahoo, M. Mikolášek, K. Hušeková, E. Dobročka, J. Šoltýs, P. Ondrejka, M. Kemény, L.
444   Harmatha, M. Mičušík and K. Fröhlich, *ACS Appl. Energy Mater.*, 2021, **4**, 11162-11172.

445 24. Gurudayal, J. W. Beeman, J. Bullock, H. Wang, J. Eichhorn, C. Towle, A. Javey, F. M. Toma, N.
446   Mathews and J. W. Ager, *Energy Environ. Sci.*, 2019, **12**, 1068-1077.

447 25. S. Chu, P. Ou, P. Ghamari, S. Vanka, B. Zhou, I. Shih, J. Song and Z. Mi, *J. Am. Chem. Soc.*,
448   2018, **140**, 7869-7877.

449 26. A. Bagger, W. Ju, A. S. Varela, P. Strasser and J. Rossmeisl, *ChemPhysChem*, 2017, **18**, 3266-
450   3273.

451 27. D. Gao, R. M. Arán-Ais, H. S. Jeon and B. Roldan Cuenya, *Nat. Catal.*, 2019, **2**, 198-210.

452 28. C. W. Lee, C. Kim and B. K. Min, *Nano Converg.*, 2019, **6**, 8.

453 29. J. C. Bui, C. Kim, A. J. King, O. Romiluyi, A. Kusoglu, A. Z. Weber and A. T. Bell, *Acc. Chem.*
454   *Res.*, 2022, **55**, 484-494.

455 30. C. Kim, J. C. Bui, X. Luo, J. K. Cooper, A. Kusoglu, A. Z. Weber and A. T. Bell, *Nat. Energy*,
456   2021, **6**, 1026-1034.

457 31. C. Kim, L.-C. Weng and A. T. Bell, *ACS Catal.*, 2020, **10**, 12403-12413.

458 32. D. Bae, T. Pedersen, B. Seger, M. Malizia, A. Kuznetsov, O. Hansen, I. Chorkendorff and P. C.
459   K. Vesborg, *Energy Environ. Sci.*, 2015, **8**, 650-660.

460 33. S. Wang, T. Wang, B. Liu, H. Li, S. Feng and J. Gong, *Natl. Sci. Rev.*, 2020, **8**.

461 34. J. Zhang, C. D. Sewell, H. Huang and Z. Lin, *Adv. Energy Mater.*, 2021, **11**, 2102767.

462 35. S. Avasthi, W. E. McClain, G. Man, A. Kahn, J. Schwartz and J. C. Sturm, *Appl. Phys. Lett.*, 2013,
463   **102**, 203901.

464 36. A. Agrawal, J. Lin, M. Barth, R. White, B. Zheng, S. Chopra, S. Gupta, K. Wang, J. Gelatos, S.

465   E. Mohney and S. Datta, *Appl. Phys. Lett.*, 2014, **104**, 112101.

466   37.   D. Connelly, C. Faulkner, P. A. Clifton and D. E. Grupp, *Appl. Phys. Lett.*, 2006, **88**, 012105.

467   38.   W. Mönch, *J. Appl. Phys.*, 2012, **111**, 073706.

468   39.   O. J. Alley, K. Wyatt, M. A. Steiner, G. Liu, T. Kistler, G. Zeng, D. M. Larson, J. K. Cooper, J. L.
469   Young, T. G. Deutsch and F. M. Toma, *Front. Energy Res.*, 2022, **10**, 884364.

470   40.   A. J. King, A. Z. Weber and A. T. Bell, *ACS Applied Materials & Interfaces*, 2023, **15**, 23024-
471   23039.

472   41.   R. P. Antony, M. Zhang, K. Zhou, S. C. J. Loo, J. Barber and L. H. Wong, *ACS Omega*, 2018, **3**,
473   2724-2734.

474   42.   P. S. Bassi, L. Xianglin, Y. Fang, J. S. C. Loo, J. Barber and L. H. Wong, *Phys. Chem. Chem.*
475   *Phys.*, 2016, **18**, 30370-30378.

476   43.   S. S. M. Bhat, S. A. Lee, J. M. Suh, S.-P. Hong and H. W. Jang, *Appl. Sci.*, 2018, **8**, 1765.

477   44.   Y. Hori, R. Takahashi, Y. Yoshinami and A. Murata, *J. Phys. Chem. B*, 1997, **101**, 7075-7081.

478   45.   X. Liu, P. Schlexer, J. Xiao, Y. Ji, L. Wang, R. B. Sandberg, M. Tang, K. S. Brown, H. Peng, S.
479   Ringe, C. Hahn, T. F. Jaramillo, J. K. Nørskov and K. Chan, *Nat. Commun.*, 2019, **10**, 32.

480   46.   L. Wang, S. A. Nitopi, E. Bertheussen, M. Orazov, C. G. Morales-Guio, X. Liu, D. C. Higgins, K.
481   Chan, J. K. Nørskov, C. Hahn and T. F. Jaramillo, *ACS Catal.*, 2018, **8**, 7445-7454.

482